Available online at www.sciencedirect.com
ScienceDirect
Catalysis Today 116 (2006) 348–353
CATALYSIS TODAY
www.elsevier.com/locate/cattod

Optically accessible channel reactor for the kinetic investigation of hydrocarbon reforming reactions

Marcello Bosco, Frédéric Vogel *

Laboratory for Energy and Materials Cycles (LEM), General Energy Department, Paul Scherrer Institut, 5232 Villigen-PSI, Switzerland

Available online 7 July 2006

Abstract

A new experimental reactor concept for studying heterogeneously catalyzed gas phase reactions was developed, which allows true surface temperature measurements along the reactor through a quartz window without affecting the flow in the reactor using IR thermography. The catalyst is coated as a thin layer onto a metal plate. The laminar flow field is similar to the one in a monolith channel. A small stream of gas can be withdrawn with a moveable capillary to measure the concentration profile in the reactor. The spatial resolution of the gas sampling is $\leq$0.1 mm. Two- and three-dimensional fluid dynamic modeling of the channel reactor was performed to check the velocity field in the channel for different operating conditions. Buoyancy forces were insignificant at the conditions studied; the parabolic inlet flow profile was maintained along the reactor channel. The heat loss by radiation from the quartz glass top surface was found to be three times larger than the heat loss by free convection. The methanation of carbon monoxide and carbon dioxide was studied at 550 and 500 °C, respectively. For these reactions nearly isothermal conditions were observed. The partial oxidation of methane, performed without diluting the feed, was also studied at 500 and 550 °C. The measured hot spots correlated well with the concentration profile measurements. Film diffusional limitations were found only significant for the oxidation reaction.

Keywords: Kinetics; Hydrocarbon reforming; Experimental reactor; Catalytic plate; IR thermography

1. Introduction

Hydrogen is the fuel of choice for polymer electrolyte fuel cells. For mobile applications of hydrogen there are still some open issues, such as the missing fuel infrastructure. This makes on-board fuel processors with liquid fuels attractive for producing hydrogen for fuel cell vehicles. The autothermal reforming of gasoline provides an efficient method to produce hydrogen [1,2]. Mizsey and Newson [3] compared different vehicle power trains. A gasoline reformer—fuel cell power train reached a ''Well-to-wheel'' efficiency of 25%, compared to 18% for a gasoline ICE power train. The link-up of a bench scale ''shift-less'' gasoline fuel processor to a polymer electrolyte fuel cell was demonstrated in our laboratory [4]. To control a fuel processor, a simple yet accurate kinetic model is necessary. Widely used fixed-bed laboratory reactors have numerous drawbacks for the determination of the kinetics of complex reactions such as the reforming of hydrocarbons [5]. A new experimental reactor concept was developed with a laminar flow field similar to the one in a monolith channel. The catalyst is coated as thin layer onto a metal plate. Film mass transfer is the only rate influencing factor for a thin-coated catalyst surface [5]. This influence was minimized in our reactor by sampling the gas phase directly above the catalytic plate. The catalyst surface temperature was measured with IR thermography. This technique has also been applied to catalyst screening [6,7] and fixed bed temperature measurements [8]. Due to the large catalyst surface compared to the catalyst volume, an excellent heat transfer is achieved. In our system a small stream of gas can be withdrawn with a moveable capillary to measure the concentration profile in the reactor with a high spatial resolution ($\leq$0.1 mm). This represents an advantage to systems with fixed sampling points such as [9]. For a typical linear gas velocity of 0.14 m/s, this step size corresponds to a temporal resolution of $\leq$1 ms. The measurements are used to develop a kinetic model, which takes into account the complex reaction network of hydrocarbon reforming including total oxidation (TOX), partial oxidation (POX), steam reforming

* Corresponding author. Tel.: +41 56 310 2135; fax: +41 56 310 2199.
E-mail address: frederic.vogel@psi.ch (F. Vogel).

0920-5861/$ – see front matter © 2006 Published by Elsevier B.V.
doi:10.1016/j.cattod.2006.05.064

(SR), water gas shift (WGS) and methanation (MET) of CO and CO_2:

$$\text{TOX}: \quad C_nH_m + \left(n + \frac{m}{4}\right)O_2 \rightarrow nCO_2 + \frac{m}{2}H_2O, \quad \Delta H_r^0 = -802.0\,\text{kJ/mol} \ (\text{for } n = 1, m = 4) \tag{1}$$

$$\text{POX}: \quad C_nH_m + \left(\frac{n}{2}\right)O_2 \rightarrow nCO + \frac{m}{2}H_2, \quad \Delta H_r^0 = -35.6\,\text{kJ/mol} \ (\text{for } n = 1, m = 4) \tag{2}$$

$$\text{SR}: \quad C_nH_m + nH_2O \leftrightarrow nCO + \left(n + \frac{m}{2}\right)H_2, \quad \Delta H_r^0 = 206.0\,\text{kJ/mol} \ (\text{for } n = 1, m = 4) \tag{3}$$

$$\text{WGS}: \quad CO + H_2O \leftrightarrow CO_2 + H_2, \quad \Delta H_r^0 = -41.0\,\text{kJ/mol} \tag{4}$$

$$\text{MET}_{CO}: \quad CO + 3H_2 \leftrightarrow CH_4 + H_2O, \quad \Delta H_r^0 = -206.0\,\text{kJ/mol} \tag{5}$$

$$\text{MET}_{CO_2}: \quad CO_2 + 4H_2 \leftrightarrow CH_4 + 2H_2O, \quad \Delta H_r^0 = -165.0\,\text{kJ/mol} \tag{6}$$

In this paper, we report on the design issues leading to the improved reactor concept and demonstrate its benefits using the partial oxidation of methane and the methanation of carbon monoxide and carbon dioxide.

2. Experimental

2.1. Optically accessible reactor design

Fig. 1 shows a schematic sectional view of the channel reactor. The catalytic plate (C) was placed at the bottom of the reactor channel. Six heating cartridges (E) were distributed in the massive metal body of the channel reactor such that a uniform temperature distribution along the channel can be maintained. Fig. 2 shows a picture (top view) of the reactor, which was placed in an insulated box. During operation the reactor was covered with an insulating plate, which leaves open only the quartz window section. At the inlet and outlet of the reactor channel three tubes were welded to the body. The movable capillary enters the reactor through a rubber septum, at the end of the middle tube outlet (Fig. 2, right). The reactor body was made of temperature resistant stainless steel.

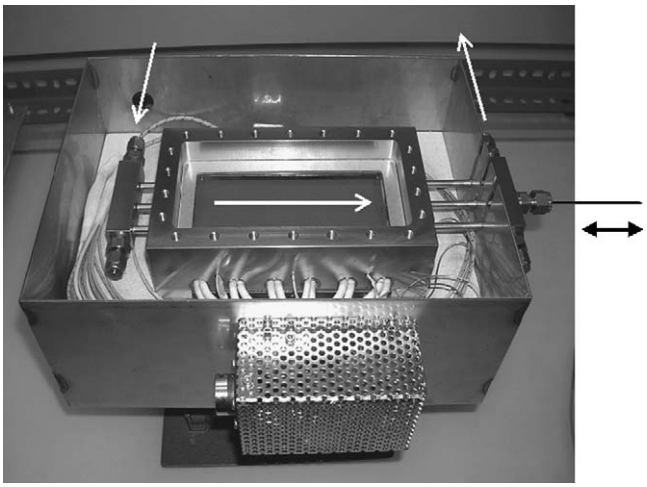

Fig. 2. Channel reactor with catalytic plate (insulation removed). The white arrows visualize the flow through the reactor. On the right hand side of the reactor the septum port with the movable sampling capillary (black arrow) is visible.

For all experiments (Table 1), the catalyst was a noble metal supported on a washcoat (total weight = 180 mg). The coated plate was provided by an industrial supplier under a secrecy agreement. The pressure for all experiments was 0.2 MPa and the weight hourly space velocity (WHSV, $g_{feed}\,g_{cat.}^{-1}\,h^{-1}$) was held between 70 and 83.

2.2. Feed system

In Fig. 3 the entire feed system (B) of the experimental setup is shown. Water and liquid hydrocarbons are fed using pressurized containers and LiquiFLOW™ (Bronkhorst) controllers, to prevent pulsations. Oxygen, methane, carbon monoxide, carbon dioxide, hydrogen, nitrogen or argon flows were controlled using mass flow controllers (Bronkhorst). Two separate evaporators for water and liquid hydrocarbons are provided. A super heater was used to heat the gas mixture to 350 °C before entering the reactor.

2.3. Surface temperature measurement

The catalyst surface temperature was measured using an infrared camera (Alpha NIR, Indigo, Fig. 3C). By using a quartz glass window the spectral range of the camera had to be

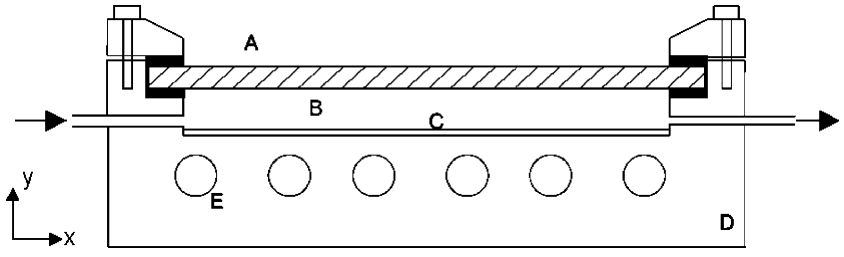

Fig. 1. Schematic side view of the channel reactor with quartz window. A, quartz window; B, gas channel; C, catalytic plate; D, reactor block; E, heating cartridges.

Table 1
Experimental parameters

Experiment	Preheater temperature (°C)	Reactor block temperature (°C)	Total inlet flow (mmol/min)	Feed concentration, $H_2/CO/CO_2/CH_4/O_2/Ar$ (vol.%)	WHSV ($g_{feed}\ g_{cat.}^{-1}\ h^{-1}$)	O/C	H_2/C
$MET_{CO}550$	350	550	7.73	30/10.5/0/0/0/59.5	70.3	–	3
$MET_{CO_2}500$	350	500	8.05	30.5/0/7.5/0/0/62	77.6	–	4
$CH_4POX500$	350	500	7.76	0/0/0/28.5/14.8/56.7	83.1	1	–
$CH_4POX550$	350	550	7.76	0/0/0/29.5/14.8/55.7	82.5	1	–

Total pressure in all experiments = 0.2 MPa (abs).

in the near infrared region. The spectral range used was 900–1700 nm. The technical specifications of the camera are: detector, indium gallium arsenide; array format, 320 × 256; pixel, 30 μm × 30 μm; frame rate, 30 Hz; temperature range, 20–1200 °C. To take into account the emissivity of the catalyst surface a calibration had to be performed. A thermocouple was placed in close contact to the catalyst surface and the reactor was heated to different temperatures until the reactor was well thermally equilibrated. A power law was fitted to the data points. After an infrared picture of the catalyst surface was taken, the measured intensities were read out along the center line of the reactor in flow direction. The temperature difference was calculated between the measured temperature of the catalyst surface during the reaction and during flushing the reactor with pure argon at constant setting of the heating system.

2.4. Gas sampling and analysis

A movable stainless steel sampling capillary, internal diameter = 0.5 mm, external diameter = 0.8 mm, entered the reactor through a high temperature septum port and was placed directly above the catalyst plate. The septum allowed the movement of the capillary during reaction without leakage up to 0.4 MPa. An electrical step motor was coupled to a linear positioning system (accuracy <0.1 mm) to automate the moving of the sampling capillary. A LabVIEW™ program controlled the step motor. The sampling capillary was connected directly to a quadrupole mass spectrometer (Prolab) for measuring the concentration of CH_4, H_2, H_2O, O_2, CO, CO_2 and Ar in the gas on-line. A heated line was connected also to a gas chromatograph (Hewlett Packard 6890) for analyzing higher hydrocarbons.

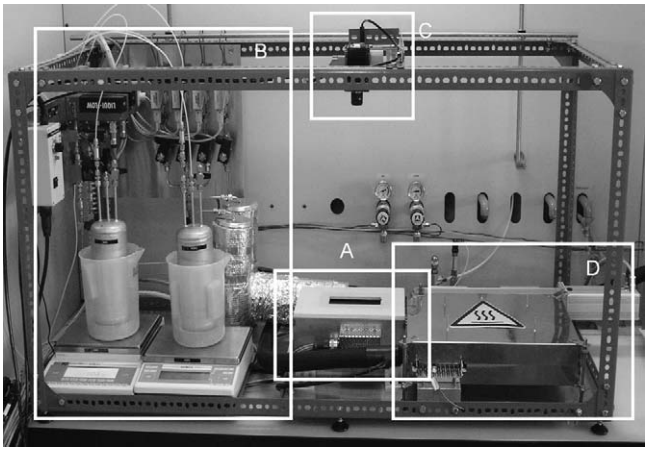

Fig. 3. Experimental setup. A, channel reactor; B, feed and preheating section; C, infrared camera; D, gas sampling system.

3. Reactor modeling

3.1. Two-dimensional and three-dimensional thermal and fluid dynamic modeling

A two-dimensional steady-state model of the channel reactor, including the heated reactor body, the catalyst coated plate, the gas channel and the quartz window, was implemented using the software FEMLAB™ (Comsol). For the fluid dynamic modeling, the time-independent Navier-Stokes equation (Eq. (7)) was solved for a flow of pure nitrogen:

$$\rho(u \cdot \nabla)u = -\nabla p + \eta\nabla^2 u + F, \qquad \nabla \cdot u = 0 \tag{7}$$

where ρ is the density (kg/m^3), η the dynamic viscosity (Pa s), and F the buoyancy force (Pa/m). The low gas velocity (typically 0.14 m/s) in the reactor made it possible to use an incompressible flow model (Mach number $\ll$1). Reynolds numbers, calculated with the hydraulic diameter $D_H = ab/[2(a+b)]$ for the rectangular (a, b) reactor channel were <30, far from the critical value ($Re_{crit.} = 2100$), and laminar flow could be expected in the reactor channel. The volume force F_y (buoyancy force, Eq. (8), which is taking into account the density changes due to a temperature difference, was also applied for the reactor channel [10]. Time-independent convective and conductive heat transport through the gas channel was modeled using Eq. (9):

$$F_y = g\rho\beta(T - T_\infty) \tag{8}$$

$$\nabla \cdot (-k\nabla T + \rho c_p T u) = Q \tag{9}$$

where c_p is the heat capacity (J/kg K) and Q the heat source (W/m^3). Conductive heat transport was also modeled for the reactor body, the catalytic plate and the quartz window (Eq. (9) with $u = 0$). For the heat transfer from the top of the quartz window to the ambient, free convection and radiation were assumed.

Temperature dependent expressions for c_p, η, k and ρ were used [11]. The temperature dependent density was calculated with the ideal gas law. For the solids, the k values were taken as constant (quartz, k = 1.46 W/m K; stainless steel, k = 20

W/m K). For the inlet a parabolic velocity profile was imposed (Eq. (10)):

$$u(y) = 6U_m \frac{y}{h}\left[1 - \frac{y}{h}\right] \quad (10)$$

where U_m is the average velocity and h the height of the gas channel. The inlet gas temperature was set to $T_{in} = 713$ K and the heating cartridges temperature was set to $T_h = 823$ K. Boundary conditions for the heat convection and conduction model were: insulated reactor body ($Q = 0$), $T_{in} = 713$ K, $T_h = 823$ K, convection $\gg$ conduction at the outlet. Since the top of the reactor is a quartz window transparent for radiation, heat loss by radiation and free convection has to be taken into account (Eq. (11)). The temperature gradient in the gas channel will be affected by the heat loss through the quartz window, which has an influence on the diffusion coefficient for the different gas species:

$$q = \alpha_c(T - T\infty) + q_{rad} \quad (11)$$

Heat loss by radiation, q_{rad}, was calculated using a band approximation and a heat balance including emission, transmission and reflexion [12]. For the free convective heat transfer from the quartz window surface to the ambient, Eqs. (12)–(14) were used to determine α_c [13]. The constants $\beta = 2.115 \times 10^{-3}$ K^{-1}, $\lambda = 38.91 \times 10^{-3}$ W/m K, $\nu = 34.94 \times 10^{-6}$ m^2/s and $Pr = 0.68$ were taken for air at an average temperature of 200 °C. The other constants were: $g = 9.81$ m/s^2, $T_\infty = 293$ K. l corresponds to the length of the quartz window:

$$Nu = 0.7(GrPr)^{1/4} \quad (12)$$

$$Nu = \frac{\alpha_c l}{\lambda} \quad (13)$$

$$Gr = \frac{gl^3}{\nu^2}\beta(T - T_\infty) \quad (14)$$

For the volumetric thermal expansion coefficient β [K^{-1}] an ideal gas was assumed. To obtain more information about the inlet section, an isothermal three-dimensional fluid dynamic model of the reactor gas channel was set up. In this model only the Navier-Stokes equation (Eq. (7)) was solved for a flow of pure nitrogen in the gas channel geometry. At the boundary of the three inlet tubes a parabolic velocity profile was assumed.

4. Results and discussion

4.1. Physical model of the channel reactor

Preliminary calculations were performed to obtain an idea of the temperature profiles and velocity profiles in the reactor channel in the absence of chemical reactions, at typical average inlet gas velocities of $U_m = 0.14$ m/s. The velocity profile exhibited no significant velocity component in y-direction. The buoyancy force, driven by the temperature difference of the hotter catalyst plate and the colder glass, had no significant effect on the velocity profile. The calculated velocity in y-direction due to the buoyancy force was a factor 1000 smaller than the velocity in x-direction. Therefore the velocity profile did not change significantly along the channel. The calculated temperature difference between the catalyst surface and the lower quartz glass surface was used to verify the absence of the Rayleigh–Bénard convection. This phenomenon is characterized by two dimensionless numbers, the Rayleigh number Ra (Eq. (15)) and the Prandtl number Pr (Eq. (16)). For our conditions Ra and Pr were 11.2 and 0.66, respectively. According to [14], these values will not lead to the formation of vertical rolls in the channel:

$$Ra = \frac{g\beta\,\Delta T h^3}{\kappa\nu} \quad (15)$$

$$Pr = \frac{\nu}{\kappa} \quad (16)$$

Due to the presence of three inlets leading into the rectangular channel, swirls may be formed at the entrance at higher flow rates. These swirls would make the data analysis and interpretation more complicated than a developed laminar flow. Fluid dynamic modeling was used to determine at which conditions swirls will occur. For the reactor inlet section a three-dimensional fluid dynamic modeling was performed. In Fig. 4 the result of the three-dimensional modeling of the upper half of the channel is shown for an inlet flow of 1 L/min. of nitrogen at 550 °C. The streamlines show the formation of eddies at the inlet. As a consequence, the catalytic coating was removed in the first 15% of the reactor inlet section in order to achieve a developed laminar flow over the coated catalyst section.

For a catalyst temperature of 550 °C the upper quartz glass surface temperature was 279 °C and the lower quartz glass surface temperature was 395 °C. The heat loss by radiation at the upper quartz glass surface was 58 W. The heat loss by free convection at the upper quartz glass surface was 18.5 W. The heat loss by radiation was thus three times larger than the heat loss by free convection. Therefore the radiative heat loss had to be taken into account for the reactor modeling. As a consequence, the temperature gradient in the gas channel became larger due to the radiation heat loss. The temperature gradient affects the temperature dependent diffusion coefficients of the different species in the gas channel.

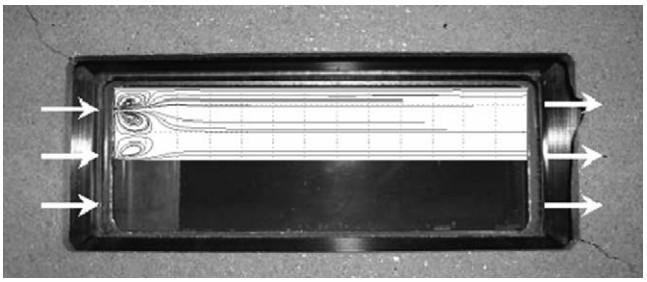

Fig. 4. Reactor top section with removed catalyst at the inlet section. Calculated streamlines (three-dimensional modeling, 1 L/min N_2 flow at 550 °C) are visible in the top section of reactor channel (white arrows show the flow direction).

4.2. Methanation experiments

In Fig. 5 the measured concentration profiles for carbon monoxide methanation at 550 °C (H_2/CO = 3) are shown together with the measured temperature difference (measured temperature on the catalyst surface during methanation subtracted by the measured temperature when flowing pure argon only). The sampling capillary was held for 1 min at the respective position shown in the graph. The concentration value was averaged over forty measurements of the mass spectrometer. The measured concentration profiles in the channel in Fig. 5 show a decrease of hydrogen upstream of the catalytic coating. This phenomenon can be explained by axial dispersion and the five times larger diffusivity of hydrogen compared to the other species. The observed effect can be seen in profile measurements in which hydrogen is present in the feed to the reactor (Figs. 5 and 6). On the catalyst coated part of the channel in Fig. 5, the concentrations of hydrogen and carbon monoxide decrease, whereas the concentrations of methane and water increase. A small amount of carbon dioxide is formed due to the water gas shift reaction involving the water formed in the methanation. Although the methanation reaction is highly exothermic, the temperature profiles are almost isothermal (maximum +5 K, Fig. 5).

In Fig. 6 the measured concentration profiles for the methanation of carbon dioxide at 500 °C (H_2/CO_2 = 4) are shown. In this experiment a small amount of water and carbon monoxide are formed upstream of the coated catalyst. The reverse water gas shift reaction could be responsible for that phenomenon. The nickel in the stainless steel may be catalytically active at those temperatures. The measured temperature difference on the catalyst surface was very small. For the methanation of carbon dioxide at 500 °C no significant temperature difference was measured (see Fig. 6). This is one of the benefits of using catalytically coated metal plates, rather than an integral fixed-bed reactor.

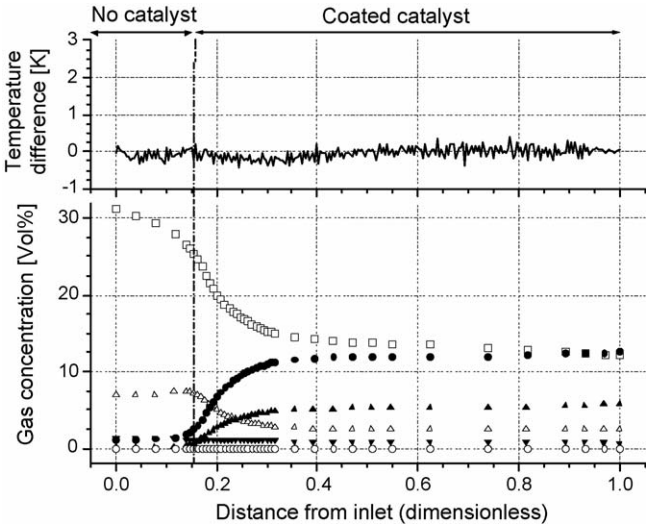

Fig. 6. Concentration profile measurement and temperature difference on the catalyst surface during CO_2 methanation at 500 °C ($MET_{CO_2}500$) with H_2/CO_2 = 4. Concentrations: CH_4 (▲), O_2 (○), H_2O (●), H_2 (□), CO_2 (△), and CO (▼).

4.3. Partial oxidation of methane

In Figs. 7 and 8 the measured concentration profiles for the partial oxidation of methane at 500 and 550 °C at an oxygen-to-carbon ratio (O/C) of 1 are plotted. No products other than CO, CO_2, H_2 and H_2O were detected in the gas phase. Oxygen is completely consumed after 35% of the reactor length at 500 °C and after 25% of the reactor length at 550 °C. In both cases the location of the measured hotspot corresponds to the decay of the oxygen. After the oxygen is consumed, no temperature difference is measured on the catalyst surface. The measured hot spots are 14 K for the experiment at 500 °C and 26 K for the experiment at 550 °C. Similar experiments conducted in a small

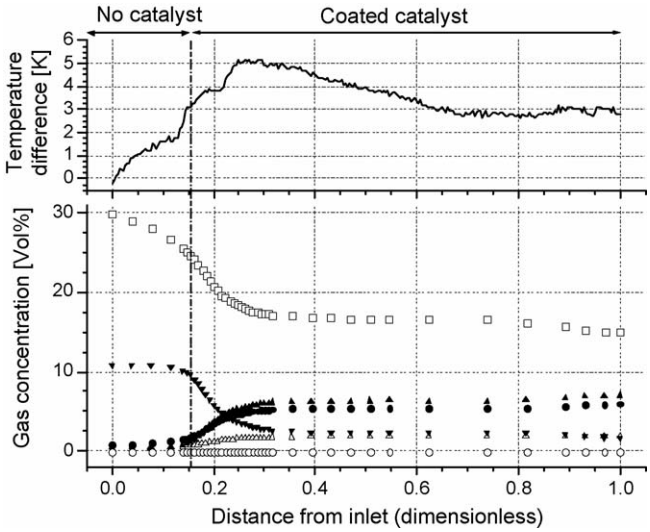

Fig. 5. Concentration profile measurement and temperature difference on the catalyst surface during CO methanation at 550 °C ($MET_{CO}550$) with H_2/CO = 3. Concentrations: CH_4 (▲), O_2 (○), H_2O (●), H_2 (□), CO_2 (△), and CO (▼).

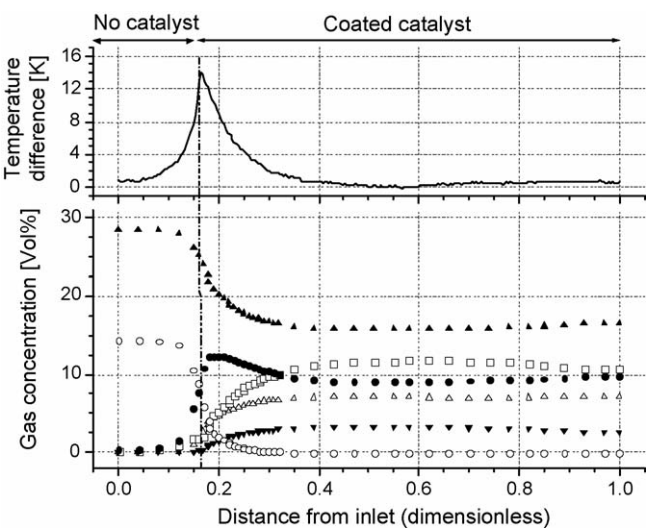

Fig. 7. Concentration profile measurement and temperature difference on the catalyst surface during partial oxidation of methane at 500 °C (CH_4POX500) with O/C = 1. Concentrations: CH_4 (▲), O_2 (○), H_2O (●), H_2 (□), CO_2 (△), and CO (▼).

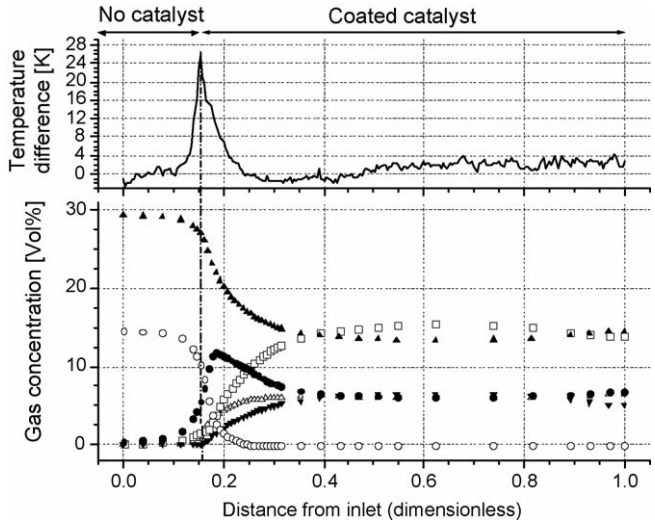

Fig. 8. Concentration profile measurement and temperature difference on the catalyst surface during partial oxidation of methane at 550 °C (CH_4POX550) with O/C = 1. Concentrations: CH_4 (▲), O_2 (○), H_2O (●), H_2 (□), CO_2 (△), and CO (▼).

fixed-bed reactor (200 mg of catalyst, particle size: 125–250 μm, diluted 1:10 with sea sand) exhibited hot spots of ≥140 K at a WHSV of 63 $g_{feed}\, g_{cat.}^{-1}\, h^{-1}$ [15].

In both experiments water is produced very fast due the total oxidation of methane. After the water concentration has reached a maximum value, the concentration decreases due to the steam reforming and water gas shift reactions. The water concentration drop at 550 °C is larger than at 500 °C due to the higher steam reforming activity at 550 °C. The measured concentration profiles indicate that carbon dioxide, carbon monoxide, hydrogen and water are primary products in the early stage (∼1 ms) of the reactions. However, due to some diffusional limitations for very fast reactions (estimated Damköhler number ca. 83 for the total oxidation of methane, calculated with rate laws from [16]), the partial oxidation of methane to carbon monoxide and hydrogen, followed by the very fast carbon monoxide and hydrogen oxidation, would probably lead to the same conclusions.

5. Conclusions and outlook

Fluid dynamic modeling of a catalytically coated channel reactor was carried out using the commercial Finite Elements package FEMLAB™. The buoyancy force had no significant influence on the velocity profile in the reactor channel. For nitrogen the parabolic velocity profile was maintained along the entire channel. The Rayleigh–Bénard convection was absent for the conditions studied. As a result of the three-dimensional fluid dynamic modeling, the catalyst coating was removed from 15% of the channel reactor length in order to have a developed laminar flow over the catalyst without eddies. The heat loss by radiation was found to be three times larger than the heat loss by free convection from the upper quartz glass surface. Due to the temperature gradient across the gas channel (150 K at 500 °C reactor temperature), the temperature dependence of the diffusion coefficients must be taken into account.

The new concept of the optically accessible channel reactor was tested with the methanation of carbon monoxide and carbon dioxide at 550 and 500 °C, respectively. The partial oxidation of methane studied at 500 and 550 °C highlighted the rapid production of water due to total oxidation of methane followed by the steam reforming and water gas shift reactions with the water formed in the total oxidation of methane.

The infrared temperature measurements of the catalyst surface showed that the channel reactor was working nearly isothermal. Even for highly exothermic reactions such as the partial oxidation of methane the measured hotspots did not exceed 25 K. The nearly isothermal behavior of the catalyst channel reactor is a major advantage for the kinetic modeling of highly exothermic or endothermic reactions with a slow to intermediate rate.

These experiments showed that gas sampling and the surface temperature measurements can be carried out with a high spatial resolution and excellent reproducibility. The benefit of the high resolution is that the concentration profiles can be measured accurately in the non-equilibrium region, even though the exit concentrations may be at equilibrium. The large amount of measured data points at different positions allows for a discrimination of similar kinetic models and reduces the uncertainty in the fitted kinetic parameters.

Acknowledgments

The authors thank P. Binkert, P. Hottinger, T. Marti, E. De Boni, J. Schneebeli and T.-B. Truong for constructional work, and T. Böhme (ETHZ), D. Ruch (ETHZ), S. Stucki and A. Wokaun for fruitful discussions.

References

[1] E. Newson, T.-B. Truong, Int. J. Hydrogen Energy 28 (2003) 1379.
[2] W.L. Mitchell, M. Hagan, S.K. Prabuhu, SAE, 1999-01-0535.
[3] P. Mizsey, E. Newson, J. Power Sources 102 (2001) 205–209.
[4] M. Bosco, F. Hajbolouri, T.-B. Truong, E. De Boni, F. Vogel, G.G. Scherer, J. Power Sources, in press, doi:10.1016/j.jpowsour.2005.12.025.
[5] O. Levenspiel, Chemical Reaction Engineering, 3rd ed., John Wiley & Sons, 1999.
[6] J. Urschey, A. Kühnle, W.F. Maier, Appl. Catal. A: Gen. 252 (2003) 91–106.
[7] A. Berkessel, E. Ashkenazi, M.R.M. Andreae, Appl. Catal. A: Gen. 254 (2003) 27–34.
[8] B. Li, K. Maruyama, M. Nurunnaabi, K. Kunimori, K. Tomishige, Ind. Eng. Chem. Res. 44 (2005) 485–494.
[9] S. Springmann, G. Friedrich, M. Himmen, M. Sommer, G. Eigenberger, Appl. Catal. A: Gen. 235 (2002) 101–111.
[10] F.P. Incropera, D.P. DeWitt, Fundamentals of Heat and Mass Transfer, 5th ed., Wiley, New York, 2002.
[11] Data compilation tables of properties of pure compounds, American Institute of Chemical Engineers, New York, 1985.
[12] D. Ruch, Autotherme Reformierung von Benzin zur Wasserstoffherstellung für Brennstoffzellen-anwendungen, Bachelor Thesis, ETH Zurich, July 2005.
[13] VDI-Wärmeatlas, 4. Auflage, VDI-Verlag GmbH, Düsseldorf, 1984.
[14] A. Bejan, Convection Heat Transfer, 2nd ed., John Wiley & Sons, 1995.
[15] S. Rabe, T.-B. Truong, F. Vogel, Appl. Catal. A: Gen. 292 (2005) 177–188.
[16] D.L. Hoang, S.H. Chan, Appl. Catal. A: Gen. 268 (2004) 207–216.